


## RESEARCH ARTICLE

Engineering Reports

Open Access

WILEY

# Mineralization based on CSAMT data: A case study on the Gaoloushan section of Yangshan gold belt

Yongling Chen<sup>1</sup> | Hu Yang<sup>1</sup>  | Chun Zhan<sup>1</sup> | Wei Zhang<sup>1,2</sup> | Jia Wang<sup>1</sup> | Dan Xie<sup>1</sup> | Wei Wei<sup>1</sup> | Ciren Lamu<sup>1</sup>

<sup>1</sup>Research Center of Applied Geology of China Geological Survey, Chengdu, China

<sup>2</sup>School of Resources and Environment, University of Electronic Science and Technology of China, Chengdu, China

## Correspondence

Hu Yang, Research Center of Applied Geology of China Geological Survey, Chengdu 610000, China.  
Email: [huyanghu61@163.com](mailto:huyanghu61@163.com)

## Funding information

Applied Geology Research Center of the China Geological Survey, Grant/Award Number: DD20220971

## Abstract

Yangshan gold belt (YSGB) in Gansu Province is a super-large orogenic gold deposit located in the middle section of the Mianxian-Lueyang arcuate suture zone (Mian-Lue suture zone). The YSGB is mainly divided into the Gejiaowan, Anba, and Gaoloushan mine sections. The ore veins are strictly controlled by strong strain zones in the fracture zone and secondary fractures superimposed on the inherited activity and are vein-like in general and lenticular in localities. For a long time, there have been different understandings regarding its ore-controlling factors and mineral genesis. By utilizing controlled-source audio-frequency magnetotellurics (CSAMT) technology to conduct electrical characteristic studies, the deep electrical structural characteristics of the Gaoloushan section are identified, and a tectonically-controlled geoelectric model of the deposit is established, which provides geophysical evidence for the view that the Yangshan gold mine is a tectonically-controlled low-temperature hydrothermal deposit in altered rock, guiding the arrangement of exploration work and identifying prospective mining areas, and thereby providing a geophysical exploration paradigm for deep exploration of large orogenic gold deposits.

## KEYWORDS

CSAMT, fault, gold deposit, Yangshan

## 1 | INTRODUCTION

The YSGB is located in the Mian-Lue suture zone of the Western Qinling Orogen, which is sandwiched among the southern edge of the Qinling microplates, the northern edge of the Yangtze Plate.<sup>1,2</sup>

YSGB in the western Qinling Mountains is located in Wen County. It is a very large independent gold deposit discovered in China so far. Since its discovery in 1997, the gold reserves have exceeded 300 tons. Yangshan gold belt (YSGB) can be divided into six ore deposits from west to east: Nishan, Getiaowan, Anba, and Zhangjiashan, with the Anba ore deposit being the core area. The unique ore-forming structural environment and complex ore-controlling factors of this gold deposit, along with the lack of geophysical data in deep areas, have hindered the understanding of the spatial distribution

This is an open access article under the terms of the [Creative Commons Attribution](https://creativecommons.org/licenses/by/4.0/) License, which permits use, distribution and reproduction in any medium, provided the original work is properly cited.

© 2024 The Author(s). *Engineering Reports* published by John Wiley & Sons Ltd.

patterns of the ore bodies. This has limited the research and exploration work in other ore segments, particularly the Gaoloushan ore segment.

To provide new directions for gold exploration in this area and address the ore-bearing structural issues in the Gaoloushan ore segment of YSGB, it is necessary to use geophysical exploration techniques to reveal key geological information, such as deep-seated concealed structures and ore-forming spaces. This will help determine the deep ore-forming action indicators under its ore-forming model, thereby providing objective technical support for the scientific deployment of exploration work. Currently.

In the exploration of Gold deposits, electromagnetic approaches were used widely. Among the most notable is the controlled-source audio-frequency magnetotelluric method (CSAMT), which brings benefits over traditional electrical approaches, including a larger range of frequency parameters and a deeper investigation depth. Because it uses artificial sources and has good signal-to-noise ratios and effective data gathering, CSAMT has been successfully utilized in the exploration of the Zhaishang Gold Deposit, Jiaodong Gold Deposit, and Nevada Gold Deposit. CSAMT is a generally used tool for mineral deposit discovery.

Zhaishang gold mine and YSGB are in the same gold deposit in the West Qinling Tectonic Belt. Liu Cheng identified the underground ore-controlling structures and inferred the location of the deep ore endowment by carrying out CSAMT work in the Zhaishang gold mine, which provided a basis for guiding the exploration of overburdened minerals in the work area. Li Hongwei has identified the electrical characteristics of the deep geological structure of the Anba mine section by using CSAMT measurements in the YSGB, which provides the basis for summarizing the ore-controlling factors and metallogenic laws in the mine area, and even the circle of ore bodies, and lays the foundation for the next step of the deep exploration.

This article uses CSAMT to conduct exploration work on the Gaoloushan ore section of the YSGB, analyzes the data through inversion, and interprets the geological and geophysical information, which shows the electrical structure of the geological body and the deep fractured alteration zone, to determine the depth of the ore body and guide the drilling work.

## 2 | GEOLOGICAL BACKGROUND

### 2.1 | Regional geology

YSGB is located in an “inverted triangle” geotectonic position between the Yangtze Plate, and the North China Plate. Its geographical coordinates are E104°29–105°00; N33°00–33°10 (as Figure 1). Mesoproterozoic to quaternary strata have formed the regional stratigraphy, which also includes the Mesoproterozoic Bikou Group, which is located in the southeast of the region in the Motianling zone. Sandstones, Dolomites, and Tufts are the majority of the shallow metamorphic volcanic-sedimentary rocks that have formed this group. A sequence of massive, clastic-eat sedimentary rocks has formed the extensively exposed Devonian strata. The Wenxian arc tectonic zone is surrounded by carboniferous fields, which are shaped by a variety of coastal carbonate sedimentary formations, primarily thick layers of stone. The Permian rocks of the region are found in the northwest and southwest and are shaped by regular sedimentary clastic rocks, which are mostly Sandstones, Dolomitic tufts, and Tufts. The research region includes rocks from the Triassic era as well, namely clastic rocks from the coast and shallow marine, with minor amounts of carbonate rocks, mostly sandstone, and sandy shale. The Puziba-Qiaotou-Moba region is home to the Jurassic series, which is mostly composed of red sandy conglomerate material. Large exposures of Quaternary alluvial deposits and Cenozoic-Tertiary loess are also present.<sup>4–6</sup>

In long-term geological activities, this orogenic belt has been influenced by multiple tectonic magmatic activities, and most of the magmatic rocks are in the form of veins, with a wide distribution range, but there are few large-scale exposed phenomena. Some scholars have found that these rocks are widely exposed, but their distribution is not concentrated. Most of them are distributed along regional faults parallel to the regional tectonic lines, and regional structures have a significant impact on their distribution. The exposed parts mainly consist of various extrusive rocks, including quartz diorite porphyry, fine-grained granite porphyry, and granite porphyry, exhibiting strong intrusive characteristics, all the evidence shows it has large-scale outcrops.<sup>3,7,8</sup>

The research area can be divided into four arc-shaped thrust tectonic zones, which are distributed in a complex manner, mainly characterized by serrated arrangements, and obvious fold structures can be observed at the top of the arc.<sup>1,2</sup> Figure 1 shows several structural belts, including Xiahe Lixian, Luqu Chengxian, and Langmusi Nanping, with similar layouts. The fold structures mainly include Lixian Xiahe, Luqu Chengxian, Diebu Zhouqu structures, and so on, and their arrangement direction is from north to south.<sup>1,2</sup>

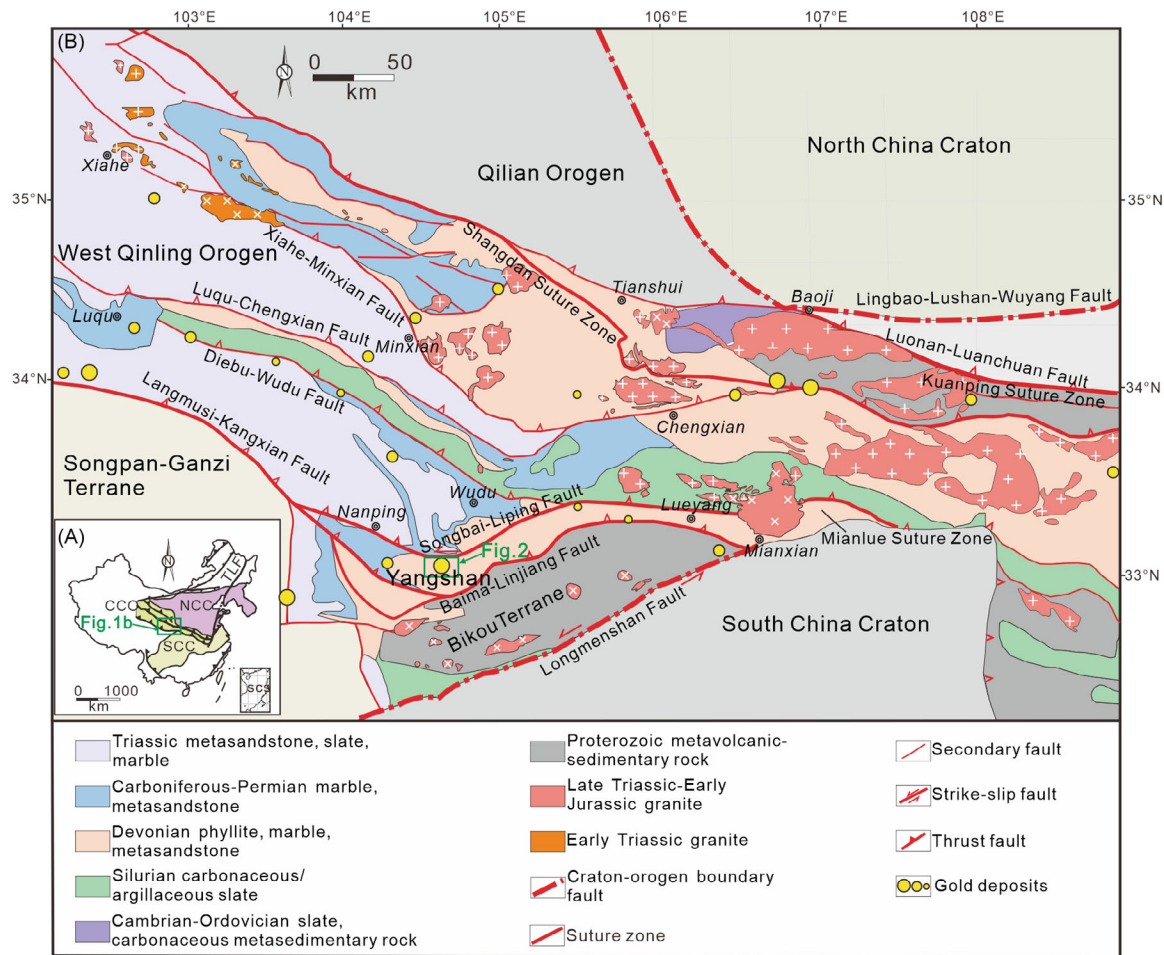


**FIGURE 1** The geological diagram of the West Qinling orogenic belt shows the distribution of crustal blocks, fault systems.<sup>3</sup> (A) The structure of the location of this mountain belt. (B) Construct a background and distribution map. CCO, central China orogen; M, cotton slips; NCB, north China block.

## 2.2 | Geology of deposits

YSGB is located in the southern section of the West Qinling Orogens, in the western portion of the Mian-Lue suture zone.<sup>3,5,7,8</sup> The gold belt is divided into six sections and stretches about 30 km from Tang-bugou in the west (see Figure 2). With the greatest verified gold reserves among them, the Anba section mineralizes around 73% of the total deposits in YSGB.<sup>9</sup>

The Anchanghe-Guanyinba fault and the Caopingliang-Getiaowan complex back-slip form the structure of YSGB, from which secondary faults, facies, lineaments, and related structures have developed.<sup>10–14</sup> The two flanks of the Caopingliang complex dip contain the majority of the ore bodies in the gold belt. The Anchanghe-Guanyinba fault and its auxiliary faults primarily regulate the distribution of these ore bodies. The composition of ore-bearing strata is very complex, mainly including components such as phyllite, fractured altered rock, limestone, and so on. The processes of hydrothermal alteration include silicification, carbonatization, and the development of chlorite, chlorite, and without any discernible spatial zonation. The strongest direct correlations are among gold mineralization, sericitization, and silicification.<sup>15–17</sup>

## 3 | DATA ACQUISITION AND PROCESSING

### 3.1 | Data acquisition

The CSAMT data of the four survey lines applied in the present research were collected by the Research Center of Applied Geology of China Geological Survey in 2022. Figure 3 shows the location of the measurement points, and the GDP-32

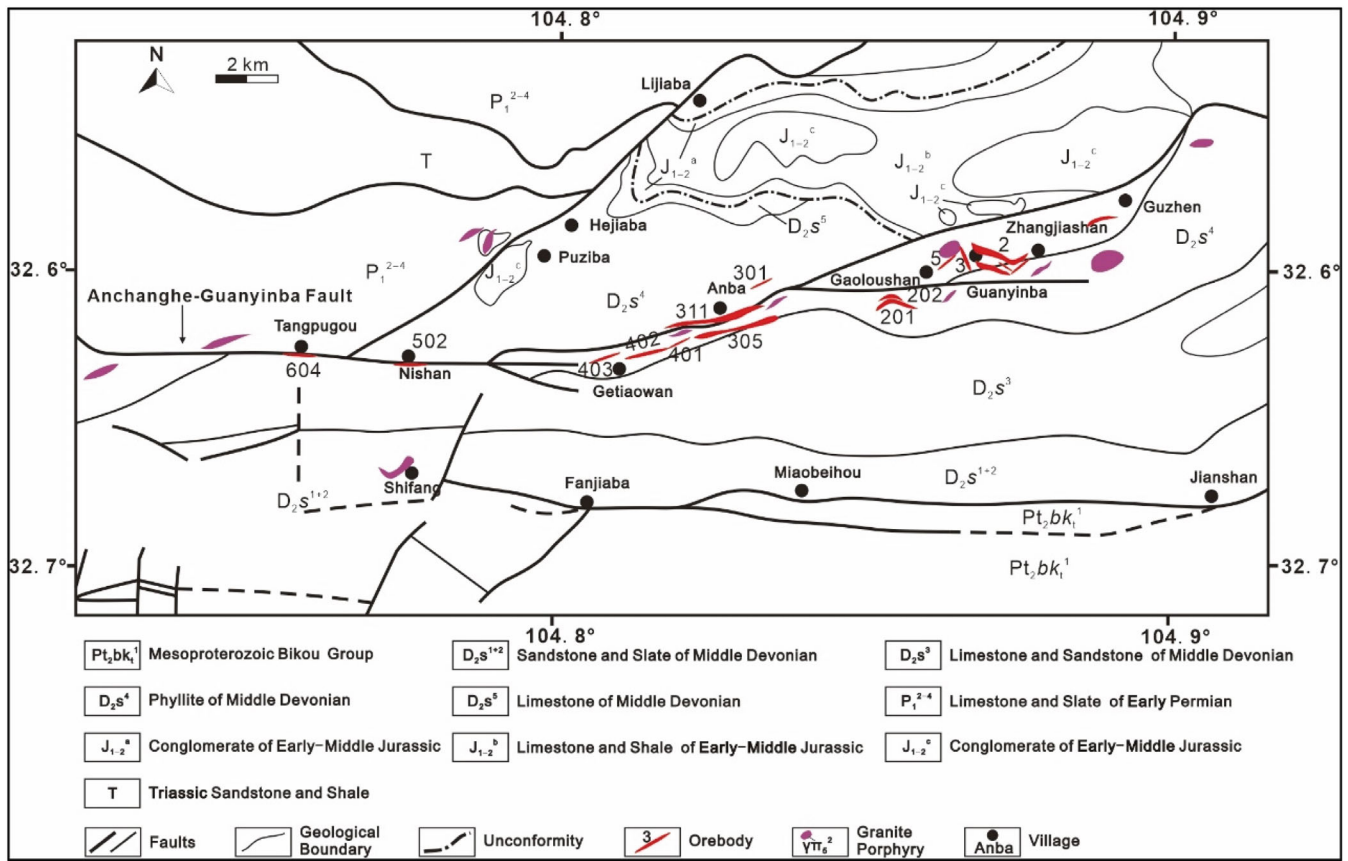


FIGURE 2 Yangshan gold belt simplified regional geology and mineral deposit geology diagram (revised based on Ref. [8]).

TABLE 1 Geophysical feature of Yangshan deposit.

Rocks	Resistivity range ( $\Omega\text{m}$ )	Resistivity average ( $\Omega\text{m}$ )
Limestone	3000–5400	3608
Phyllite	2530–4810	3057
Granite	2650–4720	3125
Ore bearing rock	303–591	431

multifunctional electrical measuring instrument (Zongge Company, Tucson, AZ, USA) was selected for detection. An electric dipole source parallel to the survey line’s direction was the source of the emission<sup>(18–20)</sup>.

From Table 1, the apparent resistivity of limestone, phyllite, and granite in the study area is greater than 2000  $\Omega\text{m}$ . The ore-bearing rocks in the crushed zone are all characterized by low resistivity, which is below 600  $\Omega\text{m}$ . Although this feature cannot be directly applied to judge ore bodies, the strength of resistivity is mainly associated with the mineral composition of the rock and its formation structure. Because rock alteration mineralization results in a low electrical resistance, by searching for low-resistivity bodies in tectonic fracture zones, it is feasible to search for hidden ore bodies.

There were 1.5 km between the electrodes and 8 km between the transmitter and receiver. An electric dipole source parallel to the detection line’s direction was the source of the emission. The frequency range of CSAMT is 1–8192 Hz, divided into 24 frequency points. The parameters of CSAMT are the orthogonal magnetic and the electric field part. These lines had survey point spacing of 40 m. The original data curve of some points on the detection line is listed in Figure 4, which suggests that the overall SNR meets the standards.



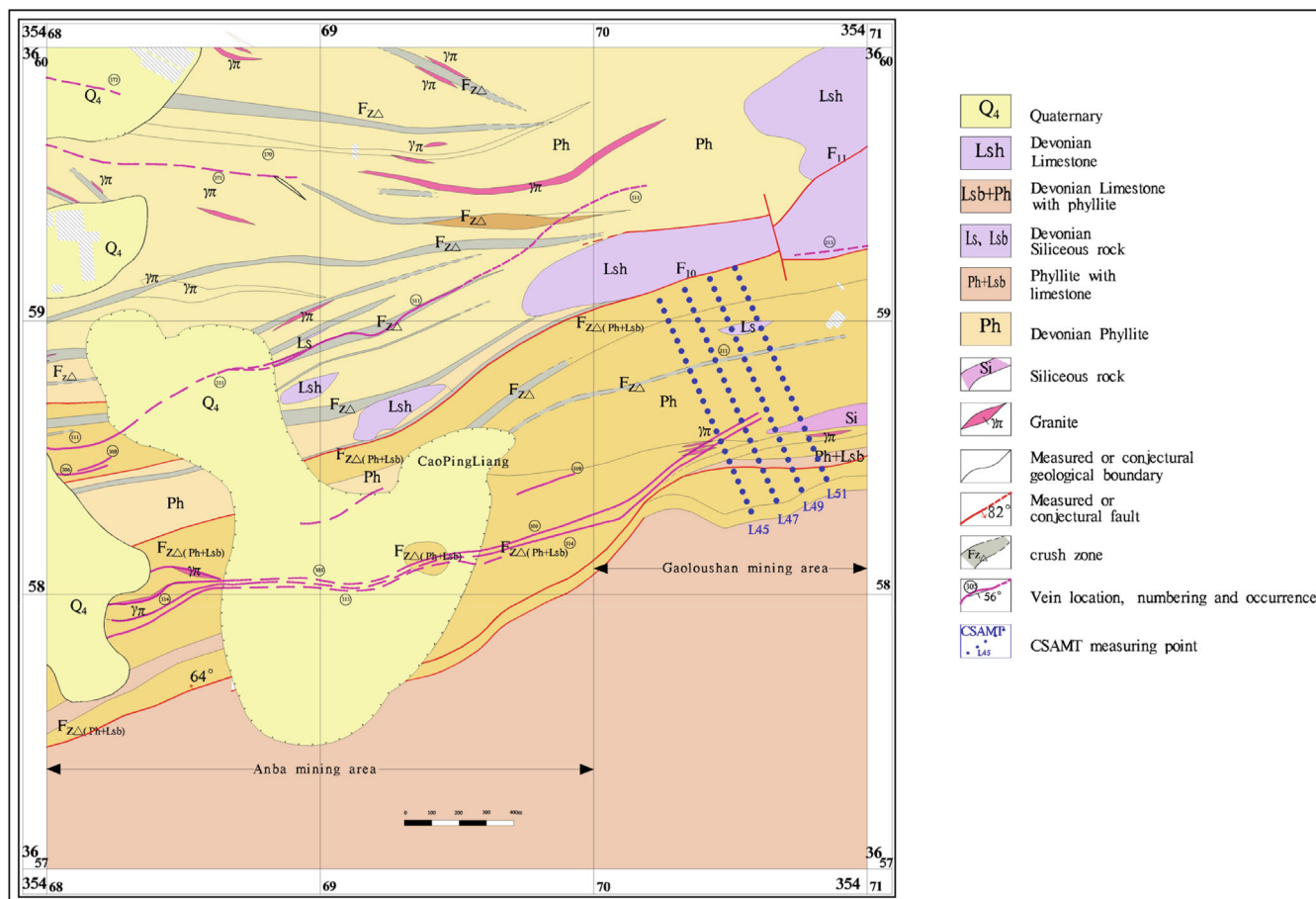


FIGURE 3 Result of the Yangshan gold deposit and relevant CSAMT profiles.

### 3.2 | Data processing and inversion

We eliminated the distorted data points and carried out the static adjustments while taking into account any interference from anthropogenic electromagnetic signals in addition to static and source effects. The areas of near-field, transition zone, and far-field were identified from the gathered data. The near-field source interference significantly disrupted frequencies lower than 10 Hz. As a result, only data between 10 and 8192 Hz were used for the inversion procedure, and these frequencies were chopped out.<sup>21,22</sup>

The static effect is a phenomenon in which the entire branch of the audio magnetotelluric sounding curve is shifted by a constant coefficient due to the additional electric field on the surface of a shallow electrical inhomogeneity, resulting in a distortion of the resistivity structure of the sounding profile. Static correction methods mainly include spatial domain filtering and curve shifting. Spatial domain filtering is generally used under simple geo-electrical conditions with better effect and is easy to cause resolution degradation when used under complex geo-electrical conditions. Curve shifting is widely applicable to all geo-electrical conditions, and in practice, it mainly follows the principles of “similarity of measurement areas” and “similarity of adjacent measurement points” to discriminate. In this static correction, the curve-shifting method is utilized. Figure 5 is a comparison of the proposed section of apparent resistivity before and after the static correction of the audio magnetotelluric sounding profile in the work area, showing that the static effect of the sounding profile is effectively removed, and the deep geological information is further highlighted through curve shifting static correction.

This article applies SCS2D software and the 2D Occam algorithm for two-dimensional inversion of collected data. In the field of geological electromagnetic data inversion, the Occam algorithm is widely used, which belongs to a smooth model-constrained inversion method.<sup>23</sup> Organize the inversion results, and Figure 6 shows the RMS mismatch of the inversion. According to the results of this graph, it can be seen that all RMS inversion residuals significantly decrease

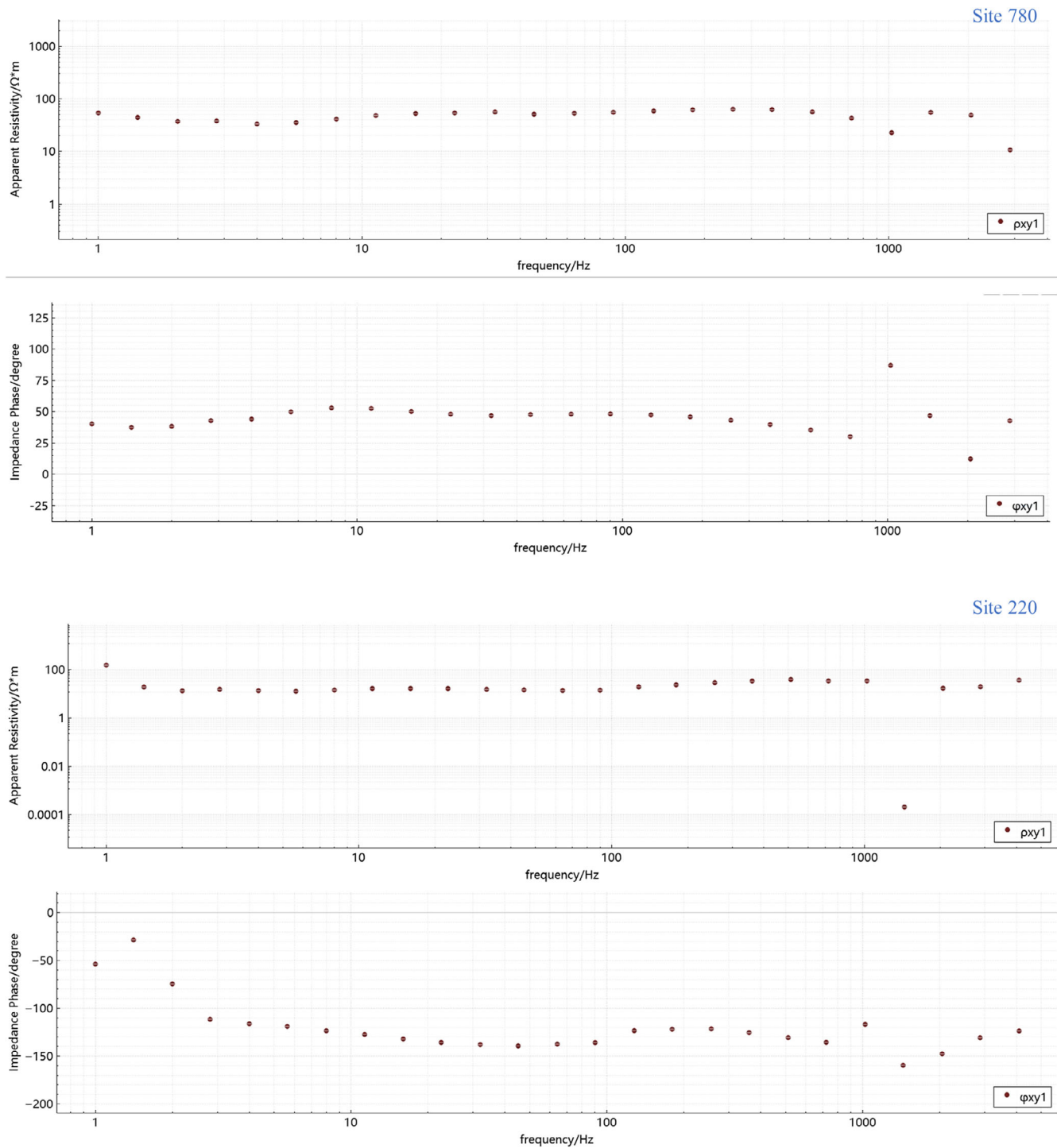


**FIGURE 4** Pseudo-sections of apparent resistivity and phase for the profile L41.

during iteration and then tend to stabilize. During the fourth iteration, the 15 curves of the contour changed very little. When the residual change rate is below 5%, end the inversion and output the result.

The inversion results can be seen from Figures 7 to 10. According to Table 1, it can be indicated that the ore-bearing rock exhibits lower resistivity. On the contrary, the limestone, phyllite, and granite are a bit higher compared with ore-bearing rock in resistivity. According to Figure 6, resistivity greater than  $1500 \Omega m$ , is a general display of granite, limestone, and phyllite. The low-resistivity anomaly between stations 350 and 500, which inferred the existence of the fault, is a conduit for hydrothermal rise and is a favorable area for mineralization.

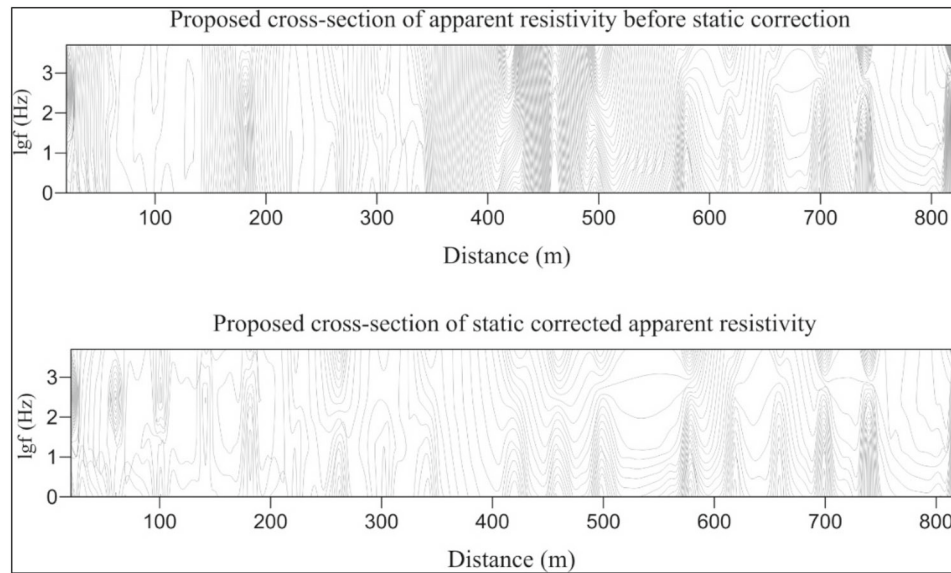


FIGURE 5 Comparison of before and after static calibration of the bathymetric profile.

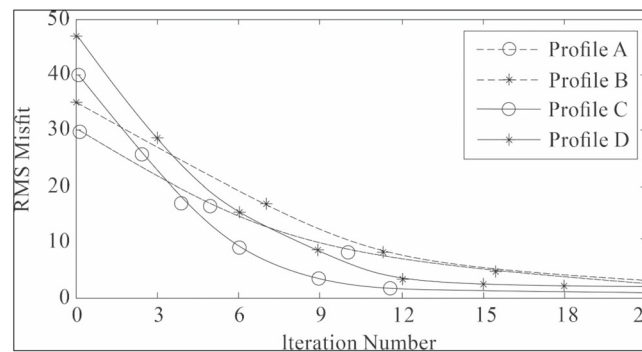


FIGURE 6 The RMS misfit of controlled-source audio-frequency magnetotellurics data inversion.

In Figures 8–10, the fault F2 is still Triassic. The resistivity in stations 400 and 750 with a depth of 300 m is very low. The high resistivity anomalies in it are probably the existence of the limestone, the phyllite, and the granite in this area.

### 3.3 | CSAMT results and interpretation

To demonstrate the distribution of resistivity in space, resistivity forms slices as exhibited in Figure 10. These slices exhibit clear layering and uniform thickness, varying with the terrain relief. The high-resistivity coverage in the northern section is continuous and in the southern section, it is discrete and thinner. In the northern and southern sections of the profile, there are two high-resistivity bodies. According to the resistivity model, the depth of their top interfaces is equal, suggesting they were originally continuous high-resistivity layers but later interrupted by low-resistivity structures.

As shown in Figure 10, profiles 45–51 display anomalies of low-resistivity structures, with clear boundaries between the high and low-resistivity zones. Therefore, this low-resistivity zone is likely composed of a tectonic fractured and altered zone caused by the Anchanghe-Guanyinba fault. It is located at a depth of 300 m between points 350 and 750, with the low-resistivity zone dipping about 40° northward.

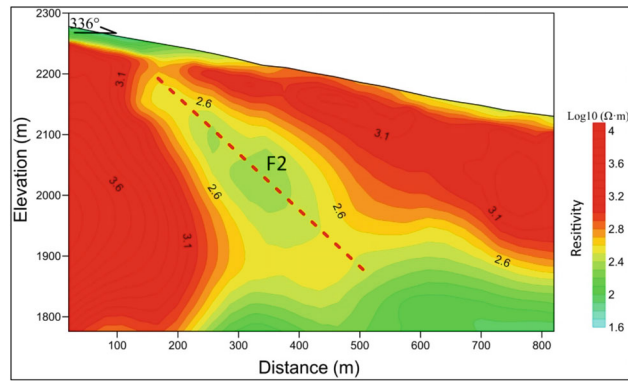


**FIGURE 7** The inversion result of 45 profile, in which distance equals to station number. The red dashed line has corresponded to fault F2.

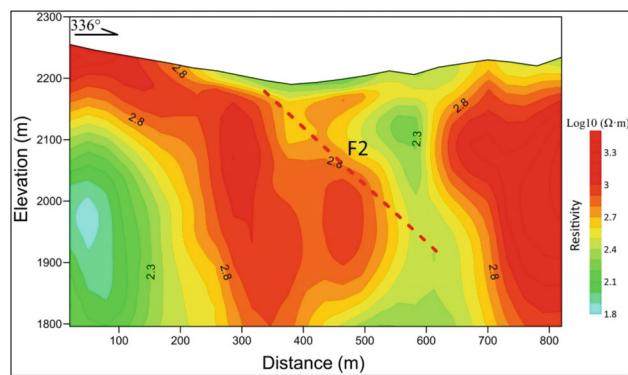


**FIGURE 8** The inversion result of 47 profile, the meanings of relevant symbols are the same as those in the above figure.

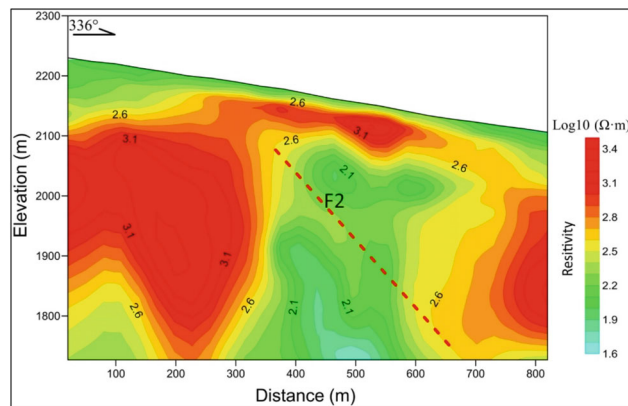


**FIGURE 9** The inversion result of 49 profile, the meanings of relevant symbols are the same as those in the above figure.

According to the mineralization model of the YSGB, hydrothermal metamorphic metallogenic fluids migrated upwards and its secondary structures, reacting with the highly permeable surrounding rocks, leading to changes in physical–chemical conditions and element migration, ultimately resulting in the precipitation of gold-bearing sulfides.

Therefore, based on the inversion results, some target areas within the study area have been delineated (Figure 11).

The illustration of the inversion of profile 49 can be seen from Figure 12. The red anomaly refers to the Gold ore body in Figure 11B, which was confirmed based on the drilling well.



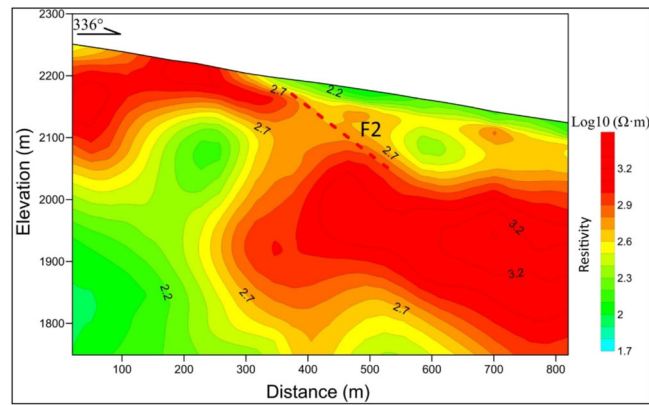


**FIGURE 10** The inversion result of 51 profile, the meanings of relevant symbols are the same as those in the above figure.

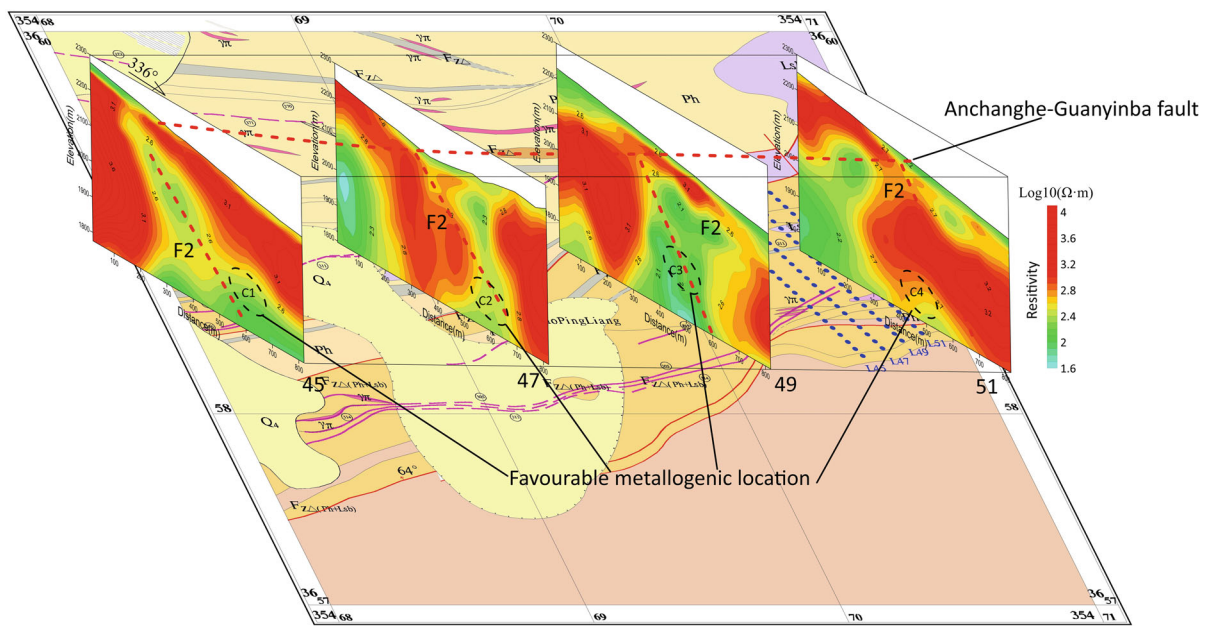


**FIGURE 11** Resistivity profiles of controlled-source audio-frequency magnetotellurics data inversion.

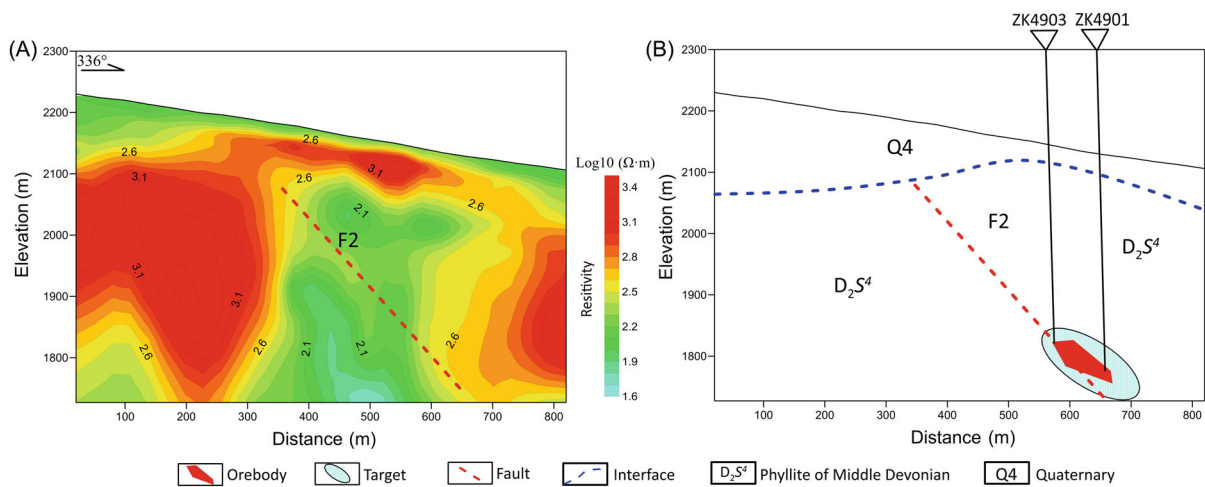


**FIGURE 12** The inversion result (A) and interpretation (B) of A profile.

## 4 | DISCUSSION

The ore-controlling structure of YSGB is a partial brittle fracture developed based on ductile deformation and facies replacement formed by the subduction collision of the Yangzi Plate to the North China Plate in the Middle and Late Triassic, which inherits the tectonic dynamics of the collision period, and the kinematic characteristics of the fracture are characterized by the retrograde thrusting from the north to the south, and the conditions for the development of the ore-bearing structures are independent of the lithologies, and the development of the mineral-bearing structures is unselective, and it can be developed in any lithologies. So, the difference in rock mechanical properties of different lithologies affects the form of tectonic development and deformation intensity, and lithology only indirectly affects the degree of development of mineral-bearing tectonics.<sup>18,19,24–27</sup>

According to the viewpoint of tectonic control at the end of hydrothermal deposit mineralization, the crystallization and precipitation of mineralized material and the aggregation of the mineralized body are mainly developed at the end of the fracture and the end of the fault.<sup>28,29</sup> Combined with the viewpoints of the above-mentioned predecessors, the fault in Figure 10 is a rising tunnel for ore-bearing fluid, and the gentle position of the fault contacting the high-resistance body of the upper plate is a favorable area for mineralization.<sup>30–32</sup>

Gold veins appeared in 3 boreholes (ZK4501, ZK4901, and ZK4903) arranged in that region, which verified our inference. Therefore, in the next step of the exploration work, priority can be given to the detailed investigation of the favorable mineralization area shown in Figure 12.

## 5 | CONCLUSIONS

The Gaoloushan mine section of YSGB has potential prospects for gold exploration. Surveys are conducted on the ore and an obvious feature of high resistivity in the ore is discovered. To analyze the electrical structure of mineralization zones, CSAMT is conducted. The 2D resistivity profiles determined based on the CSAMT survey reveal the fault existed. The former known geological data of mineral resources in the research area, combined with the CSAMT data, a few target regions are identified. To confirm the reliability of target regions, drillings were designed to clarify that, which showed a result in line with the CSAMT profiles' resistivity feature, further verifying the target zones' precision. It also provides a geophysical basis for the view that the Yangshan gold mine is a low-temperature hydrothermal deposit in altered rocks under tectonic control.

Therefore, CSAMT method is effective and can achieve good resolution for geological bodies with obvious electrical differences, through the practical application in Yangshan gold mining area. It can effectively guide the geological exploration work in the mining area and has a better practical effect on the exploration work of tectonically altered gold deposits controlled by fractures.

## AUTHOR CONTRIBUTIONS

**Yongling Chen:** Conceptualization. **Hu Yang:** Conceptualization; methodology. **Chun Zhan:** Methodology. **Wei Zhang:** Methodology; formal analysis; investigation; writing – review and editing. **Jia Wang:** Validation; resources. **Dan Xie:** Validation; data curation; visualization. **Wei Wei:** Funding acquisition; project administration. **Ciren Lamu:** Project administration.

## ACKNOWLEDGMENTS

For assistance during fieldwork, we thank the Yangshan Project Team.

## FUNDING INFORMATION

This research was funded by the Applied Geology Research Center of the China Geological Survey (no. DD20220971).

## CONFLICT OF INTEREST STATEMENT

The authors declare no conflict of interest.

## DATA AVAILABILITY STATEMENT

The data that support the findings of this study are available from the corresponding author upon reasonable request.

## ORCID

Hu Yang  <https://orcid.org/0009-0009-8536-9213>

## REFERENCES

1. Dong Y-P, Santosh M. Tectonic architecture and multiple orogeny of the Qinling Orogenic Belt, Central China. *Gondwana Res.* 2016;29:1-40.
2. Dong Y-P, Zhang G-W, Neubauer E, Liu X-M, Genser J, Hauzenberger C. Tectonic evolution of the Qinling orogen, China: review and synthesis. *J Asian Earth Sci.* 2011;41:213-237.
3. Li N, Deng J, Yang L-Q, Groves DL, Liu X-W, Dai W-G. Constraints on depositional conditions and ore-fluid source for orogenic gold districts in the West Qinling orogen, China: implications from sulfide assemblages and their trace-element geochemistry. *Ore Geol Rev.* 2018;102:204-219.
4. Liang J-L, Sun W-D, Li Y-L, et al. An XPS study on the valence states of arsenic in arsenian pyrite: implications for Au deposition mechanism of the Yangshan Carlin-type gold deposit, western Qinling belt. *J Asian Earth Sci.* 2013;62:363-372.
5. Liang J-L, Sun W-D, Zhu S-Y, Li H, Liu Y-L, Zhai W. Mineralogical study of sediment-hosted gold deposits in the Yangshan ore field, Western Qinling orogen, Central China. *J Asian Earth Sci.* 2014;85:40-50.
6. Yang L-Q, Deng J, Li N, Zhang C, Ji X-Z, Yu J-Y. Isotopic characteristics of gold deposits in the Yangshan Gold Belt, West Qinling, central China: implications for fluid and metal sources and ore genesis. *J Geochem Explor.* 2016;168:103-118.
7. Liang J-L, Li J, Sun W-D, et al. Source of ore-forming fluids of the Yangshan gold field, western Qinling orogen, China: evidence from microthermometry, noble gas isotopes and in situ sulfur isotopes of Au-carrying pyrite. *Ore Geol Rev.* 2019;105:404-422.
8. Yang Z-H, Li J-Z, Xiong T, et al. Petrogenesis of the granitic dykes in the Yangshan Gold Belt: insights from zircon U-Pb chronology, petrography, and in-situ Hf isotope analysis. *Minerals.* 2023;13:718.
9. Yang Z-H, Xiong T, Gou Z-Y, Li H, Wang L. LA-ICP-MS fission track thermochronology of apatite in the Yangshan gold ore belt, southern margin of West Qinling. *Acta Geol Sin.* 2022;96:3849-3866. (In Chinese with English abstract).
10. Guo Y-Y. *Indochinese Orogenic Gold Mineralization Deposits in the Southern Belt of the West Qinling, Central China*. PhD Thesis. China University of Geosciences. 2016. (In Chinese with English abstract).
11. Lei S-B. *Tectonic and Magmatic Constraints on Mineralization and Gold Prospecting of Yangshan Gold Belt, Gansu Province*. PhD Thesis. China University of Geosciences. 2011. (In Chinese with English abstract).
12. Li H-W. Ore-controlling factors, prospecting criteria and deep metallogenic prognosis in Yangshan gold ore belt, West Qinling Mountain. *Miner Deposits.* 2018;37(1):67-80. (In Chinese with English abstract).
13. Su Q-H, Jia R, Liu X, et al. The ore-controlling structural characteristics of Yangshan gold deposit and its enlightenment for the exploration of gold deposits in Mian-Lue tectonic mélange belt, West Qinling Orogen. *Geol Bull China.* 2020;39(8):1204-1211. (In Chinese with English abstract).
14. Zhao Y, Huang Y, Yin F-G, et al. Geochemical characteristics of structural superposition halo and coupling relationship between magma-structure-mineralization in Gaoloushan segment of Yangshan gold deposit, Wenxian County, Gansu Province. *Chin J Geol.* 2024;59(2):484-497. (In Chinese with English abstract).
15. Chen B-L. Thoughts on ore-controlling structure of the Yangshan gold deposit in southern Gansu Province, western China. *Acta Geol Sin.* 2023;97(8):2512-2533. (In Chinese with English abstract).
16. Chen J, Li Z, Tian B, et al. Using the CSAMT method to predict deep mineralisation of copper and molybdenum: a case study of the Zhongxingtun area in Inner Mongolia. *China Explor Geophys.* 2020;51:203-213.
17. Chen Y-L, Jiang S-J, Xie D, et al. Deep conductive structure of Anba ore section in Yangshan gold deposit belt and its geological meaning. *China Geol Surv.* 2023;10(1):28-36. (In Chinese with English abstract).
18. Guo Z, Hu L, Liu C, Cao C, Liu J. Application of the CSAMT method to Pb-Zn mineral. *Minerals.* 2019;9:2-12.
19. Guo Z, Hu L, Liu C, Cao C, Liu J, Liu R. Application of the CSAMT method to Pb-Zn mineral deposits: A case study in Jianshui, China. *Minerals.* 2019;9:726.
20. Zhang J, Zeng Z, Zhao X, Li J, Zhou Y, Gong M. Deep mineral exploration of the Jinchuan Cu-Ni sulfide deposit based on aeromagnetic, gravity, and CSAMT methods. *Minerals.* 2020;10:168.
21. He H, Wang J, Wen W, et al. Deep structure of epithermal deposits in Youxi area: insights from CSAMT and dual-frequency IP data. *Minerals.* 2024;14:27.
22. Lv H, Xu L, Yang B, et al. Mineralization based on CSAMT and SIP sounding data: A case study on the Hadamengou gold deposit in Inner Mongolia. *Minerals.* 2022;12:1404.
23. Constable SC, Parker RL, Constable CG. Occam's inversion: a practical algorithm for generating smooth models from electromagnetic sounding data. *Geophysics.* 1987;52:289-300.
24. Cheng B, Z F-X, H G-F. Genesis and types of the Yangsha super large micro-disseminated gold deposit, Wenxian, Gansu, China. *Geol Bull China.* 2006;25(11):1354-1360. (In Chinese with English abstract).
25. Hu X, Peng R, Wu G, Wang W, Huo G, Han B. Mineral exploration using CSAMT data: application to Longmen region metallogenic belt, Guangdong Province, China. *Geophysics.* 2013;78:B111-B119.

26. Melo AT, Sun J, Li Y. Geophysical inversions applied to 3D geology characterization of an iron oxide copper-gold deposit in Brazil. *Geophysics*. 2017;82:K1-K13.
27. Zhang R, Li T. Joint inversion of 2D gravity gradiometry and magnetotelluric data in mineral exploration. *Minerals*. 2019;9:541.
28. Lee BM, Unsworth MJ, Hübert J, Richards JP, Legault JM. 3D joint inversion of magnetotelluric and airborne tipper data: A case study from the Morrison porphyry Cu–Au–Mo deposit, British Columbia, Canada. *Geophys Prospect*. 2018;66:397-421.
29. Zhou Z-J, Mao S-D, Chen Y-J, Santosh M. U-Pb ages and Lu-Hf isotopes of detrital zircons from the southern Qinling orogen: implications for Precambrian to Phanerozoic tectonics in central China. *Gondw Res*. 2016;35:323-337.
30. Qi J-Z, Yuan S-S, Li L, et al. Geological features and ore-controlling factors of the Yangshan superlarge gold deposit, Gansu Province, China. *Geol Rev*. 2003;49(1):85-92.
31. Liang W, Tao X, Tao L, et al. Geochemical characteristics of primary halo and evaluation of deep mineralization prospect of Yangshan gold deposit, Wenxian, Gansu Province. *Miner Deposits*. 2021;40(1):143-155. (In Chinese with English abstract).
32. Zhao J, Liang J-L, Ni S-J, Xiang Q-R. In situ sulfur isotopic composition analysis of Au-bearing pyrites by using Nano-SIMS in Yangshan gold deposit, Gansu Province. *Miner Deposits*. 2016;35(4):653-662. (In Chinese with English abstract).

**How to cite this article:** Chen Y, Yang H, Zhan C, et al. Mineralization based on CSAMT data: A case study on the Gaoloushan section of Yangshan gold belt. *Engineering Reports*. 2024;6(12):e12961. doi: 10.1002/eng2.12961